Hindawi
Advances in Materials Science and Engineering
Volume 2019, Article ID 8573451, 15 pages
https://doi.org/10.1155/2019/8573451

*Research Article*

# Aminopropyl Functionalised MCM-41: Synthesis and Application for Adsorption of Pb(II) and Cd(II)

**Pham Dinh Du**,[1] **Nguyen Trung Hieu**,[2] **Thuy Chau To**,[1] **Long Giang Bach**,[3] **Mai Xuan Tinh**,[4] **Tran Xuan Mau**,[4] **and Dinh Quang Khieu**[4]

[1]*Faculty of Natural Science, Thu Dau Mot University, Thu Dau Mot 590000, Vietnam*
[2]*Center for Scientific Research and Practice, Thu Dau Mot University, Thu Dau Mot 590000, Vietnam*
[3]*NTT Institute of High Technology, Nguyen Tat Thanh University, Ho Chi Minh City 700000, Vietnam*
[4]*University of Sciences, Hue University, Hue 530000, Vietnam*

Correspondence should be addressed to Dinh Quang Khieu; dqkhieu@hueuni.edu.vn

Received 21 November 2018; Accepted 4 February 2019; Published 19 February 2019

Academic Editor: Peter Majewski



This paper shows a comparison of porous properties of aminopropyl-MCM-41 materials functionalised via the direct and indirect methods. The obtained materials were characterised using X-ray powder diffraction (XRD), transmission electron microscopy (TEM), thermogravimetric analysis-differential scanning calorimeter (TGA-DSC), adsorption/desorption isotherms of nitrogen, and Fourier-transfer infrared (FT-IR) spectroscopy. The results showed that the direct method provided the aminopropyl-MCM-41 material with well-ordered pores and high surface areas but with a lower quantity of grafted 3-aminopropyltriethoxysilane than the indirect method. To remove the organic template in the indirect method, solvent extraction with $HCl/C_2H_5OH$ and calcination at 500°C were used, and the former gave a higher quantity of grafted 3-aminopropyltriethoxysilane in the resulting aminopropyl-MCM-41 materials. The experimental data were applied to the isotherm models of adsorption including Langmuir, Freundlich, Redlich–Peterson, and Sips either in the linear or nonlinear form. In order to avoid the bias of the determination coefficient and the error function method, the paired-samples *t*-test as an alternative method was first proposed to look for the most appropriate adsorption isotherms. The maximum adsorption capacity of Cd(II) and Pb(II) was 14.08 $mg \cdot g^{-1}$ and 64.21 $mg \cdot g^{-1}$, respectively. The mechanism of complexation and isoelectric interaction was suggested to explain the adsorption of Pb(II) and Cd(II) from aqueous solutions on aminopropyl functionalised MCM-41 in the range of pH from 2 to 9.

## 1. Introduction

Lead and cadmium are potentially toxic metals released to the environment because of its wide use in many industrial applications such as metallurgy, storage battery, printing, pigments, electronics, photographic materials, and petroleum refining industry [1]. Aquatic wastewater polluted with lead and cadmium has endangered the environment and human health. The adverse effects of their toxicity include impaired blood synthesis, hypertension, severe stomach ache, brain functions and kidney damage [2], and serious osteoporosis-like bone disease [3]. A great deal of interest in the research of removing potentially toxic metals such as lead, cadmium, nickel, and mercury from industrial effluents has focused on using the adsorption approach among different other conventional removal methods [4–6]. The adsorbents have widely used to be natural and synthesised materials with large porosity and high adsorptive site density and surface area. Among porous materials, MCM-41 (Mobil Composition of Matter No. 41) is a mesoporous material with a hierarchical structure from a family of silicate that was first developed by researchers at Mobil Oil Corporation [7], and MCM-41 has received great interest because it possesses a highly ordered hexagonal structure and large specific surface area [8, 9]. Recently, the preparation of organic-inorganic hybrid silicon materials has drawn many

researchers' attention [10–12]. Surface modification by organic functional groups can improve the physical and chemical properties of the silica surface of MCM-41 and extends the practical applications of the material in catalysts [13–17] and adsorption [18, 19]. Amino groups can be included by postsynthesis grafting or by co-condensation during the synthesis [10, 11, 13–19]. In postsynthesis grafting, a precalcined mesoporous silica, partially rehydrated to generate surface hydroxyls, reacts with an appropriate alkoxysiloxane, whereas cocondensation involves the addition of both tetraethyl orthosilicate (TEOS) and a functionalised siloxane $(MeO)_3$-Si-X to the synthesis mixture.

Several models including kinetics [20], isotherm [21–28], and diffusion ones [20] have widely employed to interpret the adsorption processes. The fitting of the experimental data to these models have been carried out by various error functions such as the correlation coefficient ($r$), coefficient of determination ($r^2$), nonlinear Chi-square ($\chi^2$) test analyses, relative standard deviation [2, 24–29], Akaike's information criterion (AIC) [30], sum of the squares of errors (SSE), hybrid fractional error function (HYBRID), Mardquardt's percent standard deviation (MPSD), average relative error (ARE), and sum of the absolute errors (SAE) [31] to find out which one is the best fit. There are two approaches to choose the model: (i) compare the test value: the smaller the $\chi^2$ or AIC value, the more compatible the model is or the more the value of $R$ or $R^2$ goes to unite the best and (ii) address the question statistically and get answer in terms of probabilities. For the former, the question seems to be easy. However, the problem is how to evaluate which model is compatible when both test values are approximately the same, nor does it mention how big or small the test value is to except. This might lead to misunderstand the adsorption mechanism. For the latter, the answer is based on the statistical hypothesis testing. First, set the significant level (alpha) and if $p$ value is less than this alpha, the alternative mode fits the data significantly better than the null hypothesis model. Otherwise, accept the simpler (null) model. To the best of our knowledge, very few studies use statistical evaluation to consider the differences between the two models.

In this paper, 3-aminopropyltriethoxysilyl functionalised MCM-41 materials (denoted as aminopropyl-MCM-41) were prepared via direct and postsynthesis grafting. For the former method, aminopropyl-MCM-41 was prepared by means of direct co-condensation of 3-aminopropyltriethoxysilane and tetraethyl orthosilicate. For the latter, the amino groups were grafted to parent MCM-41 materials in which the template was removed using acid/ethanol extraction or calcination. The physical chemistry of the obtained materials was discussed. The resultant 3-aminopropyltriethoxysilane-modified MCM-41 was used as an adsorbent to remove ionic Pb(II) and Cd(II) from aqueous solutions. The isotherm models including Langmuir, Freundlich, Redlich–Peterson, and Sips in the linear and nonlinear forms were applied to describe the experimental data. In this paper, the method of paired-samples $t$-test was proposed to assess the compatibility of the adsorption isotherm models on the statistical perspective.

## 2. Experimental

*2.1. Preparation of MCM-41 and Aminopropyl-MCM-41.* Tetraethyl orthosilicate ($Si(OC_2H_5)_4$, TEOS, Merck), cetyltrimethylammonium bromide ($C_{19}H_{42}BrN$, CTAB, Merck), and 3-aminopropyltriethoxysilane ($H_2N(CH_2)_3Si(OC_2H_5)_3$, APTES, Merck) were used as a silica source, template, and functionalizing agent, respectively. Aminopropyl-MCM-41 was prepared via direct and postsynthesis grafting. For the direct synthesis, 0.5 g of CTAB, 480 mL of distilled water, and 7 mL of 2 M NaOH were mixed at 80°C for 30 minutes. Then, 9.4 g of TEOS was added to the resulting mixture under strong stirring for 30 minutes. Next, APTES with a molar ratio of TEOS/APTES = 5 was added under vigorous stirring for 1.5 hours [17]. The obtained solids were filtered. A complete removal of the organic template could be conducted in a solvent of acid/ethanol (a mixture of ethanol (100 mL) and concentrated HCl (1 mL, 36% in weight)) for 1 hour. The samples were denoted as direct-$NH_2$-MCM-41.

In the postsynthesis, first, the MCM-41 material was synthesised as mentioned above but without APTES. The CTAB template was removed from as-synthesised MCM-41 by calcination at 500°C for 6 hours to obtain a material denoted as calcined MCM-41. The other way to remove CTAB was the acid/ethanol extraction (1 gram of as-synthesised MCM-41 was added to 200 mL of a mixture $HCl/C_2H_5OH$ (the ratio of 1 mL of HCl 36% in 100 mL of $C_2H_5OH$) and stirred at room temperature for 5 minutes) to obtain a material denoted as extracted MCM-41. Then, 0.78 mL of APTES was added to 1 gram of extracted MCM-41 in 60 mL of toluene under magnetic stirring and refluxing for 8 hours at 110°C. The samples were washed many times with distilled water (until the rinse reaches the neutral medium) and denoted as post-$NH_2$-extracted MCM-41. In a similar manner, calcined MCM-41 was hydrated for 2 hours in a desiccator containing a saturated NaCl solution at the bottom before functionalisation. This sample was denoted as post-$NH_2$-calcined MCM-41.

*2.2. Characterisation of Materials.* X-ray diffraction (XRD) patterns were recorded on VNU-D8 Advance Instrument (Bruker, Germany) using Cu K$\alpha$ radiation ($\lambda = 1.5418$ Å). The $N_2$ adsorption/desorption isotherm measurements were performed at 77 K using TriStar 3000 Micromeritics. The samples were degassed at 200°C with $N_2$ for 2 hours before setting the dry mass and data collection. Specific surface areas were calculated using the Brunauer–Emmett–Teller (BET) model. Pore size distributions were calculated using the BJH model on the desorption branch. The thermal behaviour of the samples was conducted using thermal analysis-differential scanning calorimeter (TG-DSC) on Labsys TG/DSC SETARAM. The transmission electron microscopy (TEM) micrographs were obtained using JEOL JEM-2100 operating at 80 kV. Infrared spectra (IR) were recorded on an FT-IR spectrometer using IR-Prestige-21 (Shimadzu) in the KBr matrix in the range 4000–400 $cm^{-1}$.

*2.3. Determination of the Point of Zero Charge.* The point of zero charge ($pH_{PZC}$) of the aminopropyl functionalised MCM-41 materials was determined by the solid addition method [24, 32]. 25 mL of 0.1 M NaCl was added to a series of 50 mL Erlenmeyer flasks. The initial pH ($pH_i$) of the solution was adjusted, ranging from 2 to 12 by adding either 0.1 M HCl or 0.1 M NaOH solution. Then, 0.01 g of the post-$NH_2$-extracted MCM-41 sample was added to each flask, and the mixture was shaken for 48 hours. Then, the final pH ($pH_f$) of the solution was measured. The plot represents the relation between the difference of the final and initial pH value ($\Delta pH = pH_f - pH_i$), and $pH_i$ was drawn; the point of intersection of the curve with the abscissa, at which $\Delta pH = 0$, provided $pH_{PZC}$. This process is performed similarly for the 0.01 M NaCl, 0.1 M KCl, and 0.01 M KCl solutions.

*2.4. Adsorption Experiments.* The adsorption of Pb(II) and Cd(II) ions on the aminopropyl functionalised MCM-41 material was performed in an Erlenmeyer flask (volume 100 mL): 0.01 g synthetic materials were added to a 50 mL of Pb(II) (or Cd(II)) solution, the pH value of which was adjusted with the 0.1 M HCl or 0.1 M NaOH solution; the mixture was then shaken for 4 hours. Finally, the solution was centrifuged to remove the adsorbent, and the concentration of Pb(II) or Cd(II) was determined using atomic absorption spectroscopy (AAS) by Shimadzu AA-6800 (Singapore). The removal efficiency of Pb(II) and Cd(II) was accessed.

The adsorption isotherm of Pb(II) and Cd(II) in the aqueous solution of aminopropyl-MCM-41 was studies at room temperature ($27 \pm 2^{\circ}C$). 0.05 g of aminopropyl-MCM-41 was added to the Erlenmeyer flasks containing 50 mL of the Pb(II) or Cd(II) ion of various concentrations, and the mixture was shaken for 4 hours to reach equilibrium adsorption. Then, the liquid was used to determine the remaining amount of Pb(II) or Cd(II) after removing the solid by centrifuge.

The amount of the metal ion adsorbed at equilibrium ($q_e$) was calculated according to the following equation:

$$q_e = \frac{(C_0 - C_e)\cdot V}{m}\left(\mathrm{mg}\cdot\mathrm{g}^{-1}\right), \tag{1}$$

where $C_0$ and $C_e$ ($\mathrm{mg}\cdot\mathrm{L}^{-1}$) are the Pb(II) or Cd(II) ion concentrations at the initial and equilibrium time, respectively, and $V$ (L) and $m$ (g) are the volume of the Pb(II) or Cd(II) solutions and the mass of aminopropyl-MCM-41 used, respectively.

The removal efficiency ($H$) of metal ions was calculated according to the following equation:

$$H = \frac{(C_0 - C_e)}{C_0}\,(\%). \tag{2}$$

In this work, the two-parameter equations, namely, Langmuir isotherm and Freundlich isotherm, and three-parameter equations, i.e., Redlich–Peterson isotherm and Sips isotherm, were used to analyse the adsorption equilibrium data.

The Langmuir isotherm equation [20, 21, 23, 33] is as follows:

$$q_e = q_m \cdot \frac{K_L \cdot C_e}{1 + K_L \cdot C_e}, \tag{3}$$

where $q_m$ is the maximum monolayer adsorption capacity of adsorbent ($\mathrm{mg}\cdot\mathrm{g}^{-1}$) and $K_L$ is the Langmuir constant ($\mathrm{L}\cdot\mathrm{mg}^{-1}$). The other parameters have been described before.

Different linear forms of the Langmuir isotherm are shown in Table 1.

The Freundlich isotherm is expressed by the following empirical equation [20, 21, 23, 33]:

$$q_e = K_F \cdot C_e^{1/n}, \tag{4}$$

where $n$ is the heterogeneity factor and $K_F$ is the Freundlich constant ($\mathrm{mg}^{(1-1/n)}\cdot\mathrm{L}^{1/n}\cdot\mathrm{g}^{-1}$). $n$ and $K_F$ are dependent on temperature: $n$ indicates the extent of the adsorption, and $K_F$ expresses the degree of nonlinearity between the solution concentration and the adsorption. If $n$ is greater than 1, the adsorption process is favorable [20, 33].

The linear form of the Freundlich equation is

$$\ln q_e = \ln K_F + \frac{1}{n}\cdot \ln C_e. \tag{5}$$

The Redlich–Peterson isotherm equation [22, 23, 33] is as follows:

$$q_e = \frac{K_R \cdot C_e}{1 + a_R \cdot C_e^{b_R}}, \tag{6}$$

where $K_R$ ($\mathrm{L}\cdot\mathrm{g}^{-1}$) and $a_R$ ($\mathrm{L}^{b_R}\cdot\mathrm{mg}^{(b_R-1)}$) are the Redlich–Peterson isotherm constants and $b_R$ is the exponent with a value between 0 and 1.

A linear form of the Redlich–Peterson equation is

$$\ln\left(K_R \cdot \frac{C_e}{q_e} - 1\right) = b_R \cdot \ln C_e + \ln a_R. \tag{7}$$

According to the Freundlich model (equation (4)), the adsorbed amount increases with the adsorbate concentration. This is the problem of the Freundlich model. Therefore, Sips proposed an equation similar to the Freundlich equation, but it has a finite limit when the concentration is sufficiently high [22, 33]:

$$q_e = q_{mS} \cdot \frac{K_{S1} \cdot C_e^{1/n_S}}{1 + K_{S1} \cdot C_e^{1/n_S}}, \tag{8}$$

where $q_{mS}$ is the Sips maximum adsorption capacity ($\mathrm{mg}\cdot\mathrm{g}^{-1}$), $K_{S1}$ is the Sips equilibrium constant ($\mathrm{L}^{1/n_S}\cdot\mathrm{mg}^{((1/n_S)-1)}$), and $n_S$ is a constant.

The Sips isotherm can be represented as

$$q_e = \frac{K_{S2} \cdot C_e^{b_S}}{1 + a_S \cdot C_e^{b_S}}, \tag{9}$$

where $K_{S2}$ ($\mathrm{mg}^{(1-b_S)}\cdot\mathrm{L}^{b_S}\cdot\mathrm{g}^{-1}$) and $a_S$ ($\mathrm{L}^{b_S}\cdot\mathrm{mg}^{(b_S-1)}$) are the Sips isotherm constants and $b_S$ is the Sips model exponent.

The linear form of Sips equation can be described as

$$\frac{1}{q_e} = \frac{1}{K_{S2}}\cdot\frac{1}{C_e^{b_S}} + \frac{a_S}{K_{S2}}. \tag{10}$$

The Sips and Redlich–Peterson equations contain three unknown parameters, and they are impossible to obtain

Table 1: Linear form equations of the Langmuir isotherm model.

| Isotherm | Linear form | Plot | Reference |
|---|---|---|---|
| Langmuir 1 | $1/q_e = (1/(K_L \cdot q_m)) \cdot (1/C_e) + (1/q_m)$ | $(1/q_e)$ vs. $(1/C_e)$ | [21, 25–28, 33] |
| Langmuir 2 | $C_e/q_e = (1/q_m) \cdot C_e + (1/(K_L \cdot q_m))$ | $(C_e/q_e)$ vs. $C_e$ | [20, 21, 25–28, 33] |
| Langmuir 3 | $q_e = -(1/K_L) \cdot (q_e/C_e) + q_m$ | $q_e$ vs. $(q_e/C_e)$ | [21, 25–28, 33] |
| Langmuir 4 | $q_e/C_e = -K_L \cdot q_e + K_L \cdot q_m$ | $(q_e/C_e)$ vs. $q_e$ | [21, 25–28, 33] |
| Langmuir 5 | $1/C_e = K_L \cdot q_m \cdot (1/q_e) - K_L$ | $(1/C_e)$ vs. $(1/q_e)$ | [21] |

simply by linearisation. Therefore, a minimisation procedure using the Solver function of Microsoft Excel was carried out to maximise the determination coefficient of $\ln(K_R \cdot (C_e/q_e) - 1)$ vs. $\ln C_e$ and $1/q_e$ vs. $1/C_e^{b_S}$. After maximising the $R^2$ value, the isotherm parameters were determined using the linear regression equation.

## 3. Results and Discussion

*3.1. Characterisation of Aminopropyl Functionalised MCM-41.* Figure 1(a) presents the X-ray diffraction patterns of MCM-41 and the aminopropyl-MCM-41. All the samples had a single intensive reflection at the $2\theta$ angle around 2° as is the case for typical MCM-41 materials, and this reflection is generally related to a regular pore size and an ordered pore arrangement [34]. This suggests that the mesoporous structure remained intact after amine modification. However, the intensity of peak (100) characterised for the mesostructure decreased as APTES was grafted to the silica framework. The direct-$NH_2$-MCM-41 sample still remained a higher hexagonal mesoporous structure since the (100), (110), and (200) reflections were still observed. The low intensity of (100) reflection implied a poorly ordered structure of the postsynthesis samples.

The efficiency of the incorporation of APTES into the silica framework can be studied using TG-DSC (Figure 1(b)). For the as-synthesised MCM-41 samples, a large weight loss (16.3%) in several steps corresponding to the exothermic peak in DSC at around 250°C before levelling off at around 600°C was observed. Since DSC only had an exothermic peak, the removal of the template appeared to take place through oxidative decomposition rather than evaporation (desorption). For aminopropyl-MCM-41, the endothermic peak at around 100°C can be attributed to the desorption of water from the channels of the material. The second weight loss between 300 and 600°C, together with exothermic peaks corresponds to the decomposition/oxidation of aminopropyl residues. The third weight loss around 600–800°C, which could be observed for all the samples, should relate to the release of water formed during condensation of silanols in the silica framework. It was found that post-$NH_2$-calcined MCM-41 and post-$NH_2$-extracted MCM-41 showed similar patterns of thermal decomposition with sharp exothermic peaks while the direct-$NH_2$-MCM-41 sample showed a relatively broaden exothermic peak. This evidence suggested an inconsistent incorporation of APTES into the silica framework in the direct-$NH_2$-MCM-41 material. It is assumed that the weight loss over 250°C was attributed to aminopropyl loading. The amine content of direct-$NH_2$-MCM-41, post-$NH_2$-calcined MCM-41, and post-$NH_2$-extracted MCM-41 are 10.5%, 12.8%, and 17.5%, respectively. Then, although the direct-$NH_2$-MCM-41 sample possessed higher mesoporous ordering, it had lower aminopropyl loading in comparison with those of postsynthesis. The highest aminopropyl loading in post-$NH_2$-extracted MCM-41 was possible because the surface of the silica framework in which the template was removed by solvent extraction contains a larger amount of silanol groups, as mentioned in a previous paper [19].

The existence of the amino group is further confirmed by IR spectra. The FT-IR spectra of the MCM-41 and aminopropyl-MCM-41 samples are shown in Figure 2. The sharp absorption band at 3100–3600 $cm^{-1}$ is attributed to the stretching of O-H on the surface silanol groups with the hydrogen bond and the remaining adsorbed water molecules. The absorption bands at 2920 $cm^{-1}$ and 2850 $cm^{-1}$ are ascribed to the asymmetric stretching and symmetric stretching of (–$CH_2$–), respectively, while the absorption at 1460 $cm^{-1}$ is attributed to the bending of the (–$CH_2$–) group. The absorption bands at 1051 $cm^{-1}$ and 800 $cm^{-1}$ are due to Si-O-Si and Si-O stretching vibrations, respectively. The band at 954 $cm^{-1}$ is assigned to the Si-OH stretching. The adsorption band at 1635 $cm^{-1}$ is due to the deformation vibrations of adsorbed water molecules ($\delta_{H-O-H}$). The presence of the N-H bending vibration at 690 $cm^{-1}$ and –$NH_2$ symmetric bending vibration at 1532 $cm^{-1}$, which are absent in neat MCM-41, indicates the successful inclusion of organic amine onto the silica surface [10, 17, 18].

Figure 3 shows the TEM observation of calcined MCM-41, extracted MCM-41, and aminopropyl-MCM-41 grafted via the direct and indirect process. It can be seen that the calcined MCM-41 and extracted MCM-41 samples consist of nanospherical particles of around two hundred nanometres. There are nanobubbles in the extracted MCM-41 sample. These bubbles inside the nanospherical particles possibly formed during the extraction process. The acidic solvent might corrode unstable silica inside the nanoparticles producing sub-nanobubbles. Grafting APTES into the MCM-41 framework by the direct process provided the morphology with some inclusions that possibly formed through the condensation of APTES outside the MCM-41 nanoparticles, while no inclusions and smooth surface were observed in the post-$NH_2$-calcined MCM-41 or post-$NH_2$-extracted MCM-41 samples. The inconsistent condensation of 3-aminopropyltriethoxysilane including self-condensation and condensation with the silanol group of the silica framework in direct-$NH_2$-MCM-41 explained why the DSC profile had a broad exothermic peak compared with that of postaminopropyl-MCM-41.

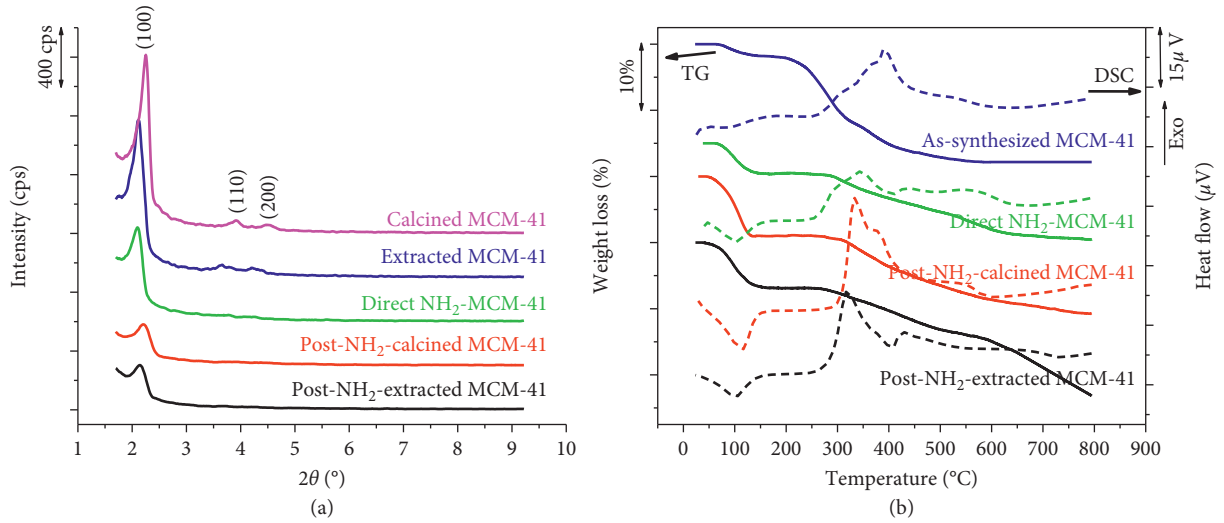


Figure 1: (a) XRD patterns of MCM-41 and aminopropyl-MCM-41; (b) TG-DSC profiles of as-synthesised MCM-41 and aminopropyl-MCM-41.

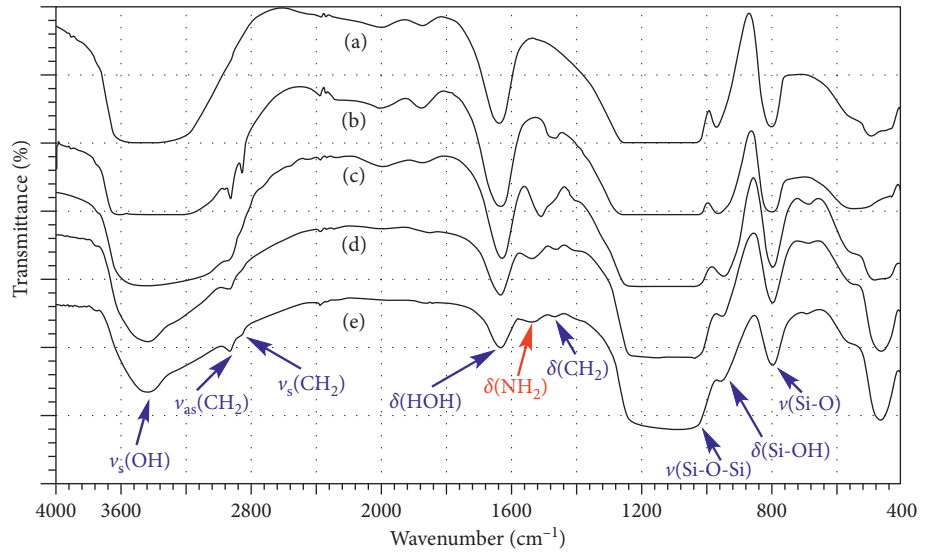


Figure 2: The FT-IR spectra: (a) calcined MCM-41; (b) extracted MCM-41; (c) direct-$NH_2$-MCM-41; (d) post-$NH_2$-calcined MCM-41; (e) post-$NH_2$-extracted MCM-41.

Figure 4 shows the nitrogen adsorption/desorption isotherms of MCM-41 and aminopropyl-MCM-41. Calcined MCM-41 and extracted MCM-41 showed practically the same porous properties. Direct-$NH_2$-MCM-41 and MCM-41 exhibited the sharp condensation capillaries around a relative pressure of 0.35 and characteristic-type IV isotherms. This shows that MCM-41 and direct-$NH_2$-MCM-41 had a hexagonal mesoporous structure with a narrow pore size distribution (the inset of Figures 4(a)–4(c)). This finding is consistent with that of the XRD study discussed in Section 3.1. A hysteresis of the $H_3$ type at $P/P_o > 0.9$ was observed for both samples prepared by postsynthesis (Figures 4(d) and 4(e)). This is due to nitrogen condensation and evaporation in the interparticle space. The distribution of the functional group on the surface of the pore wall of the materials prepared via postsynthesis was not uniform, and the organic groups could block the mesopores leading to the decrease of the surface area and broad pore distribution (Table 2 and the inset of Figures 4(d) and 4(e)).

One of the most important properties of a solid material is the point of zero charge ($pH_{PZC}$). When a solid material is in a solution with pH lower than $pH_{PZC}$, the material surface has a positive charge by adsorption of $H^+$ ions from the aqueous solution, leading to a positive variation of the solution pH ($\Delta pH > 0$). On the contrary, if the solid material is in a solution with pH greater than $pH_{PZC}$, the material surface has a negative charge by adsorption of $OH^-$ ions, leading to a negative variation of the solution pH ($\Delta pH < 0$). Thus, the pH value, at which the material surface has a zero charge, $\Delta pH = 0$, is the point of zero charge. The point of

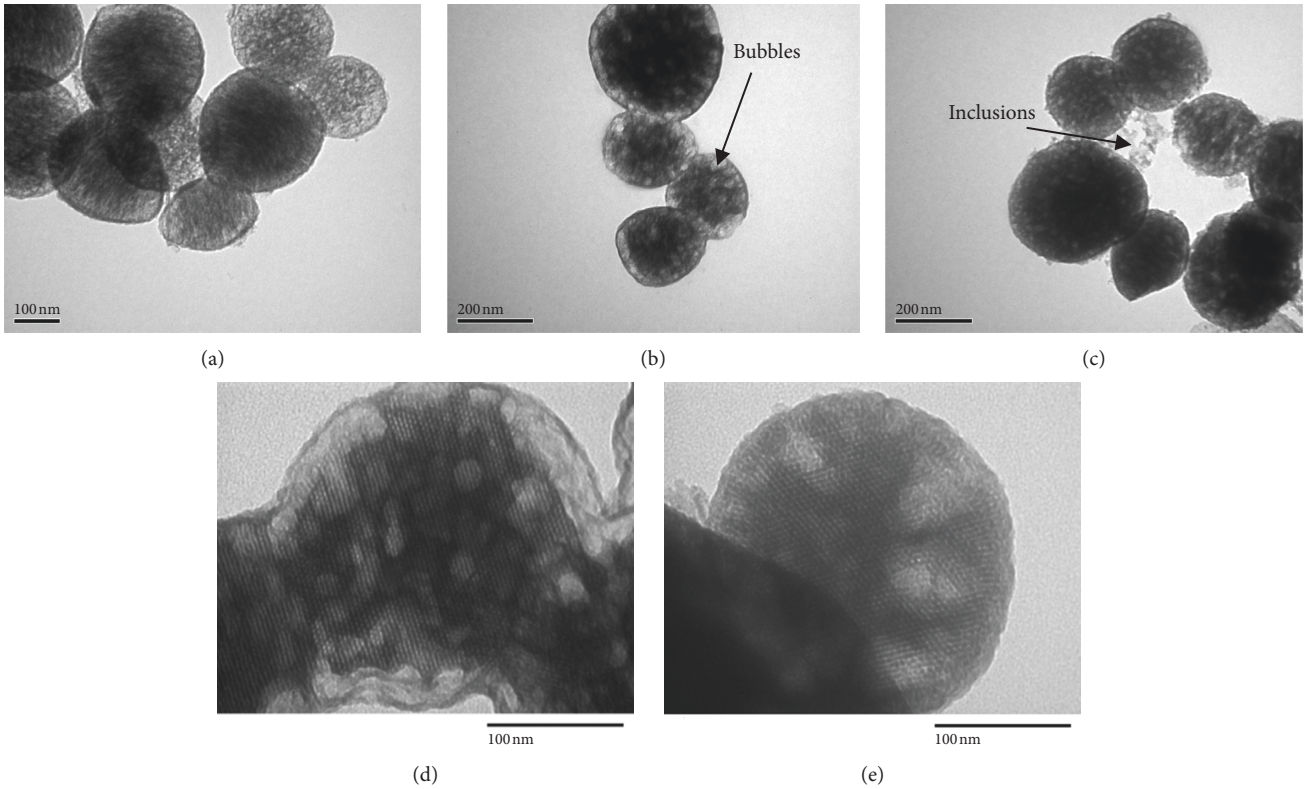


Figure 3: TEM images of MCM-41 and aminopropyl functionalised MCM-41: (a) calcined MCM-41; (b) extracted MCM-41; (c) direct-$NH_2$-MCM-41; (d) post-$NH_2$-calcined MCM-41; (e) post-$NH_2$-extracted MCM-41.

zero charge determination can be performed in a neutral environment or a neutral electrolyte solution. In this study, the NaCl and KCl solutions at two different concentrations (0.1 M and 0.01 M) were used.

The point of zero charge of the aminopropyl-MCM-41 material was 7.5 and 8.1 in the 0.1 M and 0.01 M NaCl solution, respectively (Figure 5(a)). Similarly, for the 0.1 M and 0.01 M KCl solution, the point of zero charge of the aminopropyl-MCM-41 material was 7.6 and 7.7, respectively (Figure 5(b)). It is evident that $pH_{PZC}$ of the aminopropyl-MCM-41 material was independent of the concentration of the studied electrolytes. The average value of $pH_{PZC}$ of the aminopropyl-MCM-41 material is $7.73 \pm 0.11$, which is similar to the $pH_{PZC}$ of the base solid materials already published [35]. Qin et al. [36] announced that the point of zero charge of the aminopropyl-MCM-41 material was 9.5 measured using the zeta potential. This difference is probably due to the nature of the two measurement methods and the nature of the $NH_2$-MCM-41 products.

### 3.2. Adsorption Studies

*3.2.1. Choosing Adsorbent.* The synthesised MCM-41 materials were used to adsorb Pb(II) and Cd(II) from aqueous solutions. As can be seen from Figure 6, calcined MCM-41 and extracted MCM-41 had a very low removal efficiency for Pb(II) (<20%) (Figure 6(a)) and for Cd(II) (around 7%) (Figure 6(b)). When MCM-41 was functionalised with 3-aminopropyl, it had a significantly higher removal efficiency, especially when the postsynthesis was used. For the Pb(II) adsorption, post-$NH_2$-extracted MCM-41 was more effective than post-$NH_2$-calcined MCM-41 with more than 90% efficiency as opposed to around 70%, respectively. A similar pattern of adsorption on post-$NH_2$-extracted MCM-41 and post-$NH_2$-calcined MCM-41 is seen for Cd(II) but at a much lower efficiency (20%) for both the materials. This shows that the amino group was successfully grafted to the silica wall of MCM-41. Based on these findings, post-$NH_2$-extracted MCM-41 was chosen to evaluate the adsorption capacity of the material in the further study.

*3.2.2. Effect of pH.* In order to find the dependence of the removal efficiency of the synthesised materials on the acidity of the reaction mixture, a range of pH from 2 to 9 was studied. It is clear that the removal efficiency tends to increase with the solution pH (Figure 7). At pH less than 3.5, the removal efficiency of Pb(II) and Cd(II) on aminopropyl-MCM-41 was negligible; it increased significantly in the next range of pH from 3 to 4, followed by a relatively low rise. Pb(II) was adsorbed more than Cd(II) at every pH. At pH 6, the former attained an efficiency of 65% and the latter 40%. Interestingly, Cd(II) exhibited an unusual pattern when pH continued to rise: the efficiency stayed nearly stable until pH 7 and then increased slightly at pH 8 and surged abruptly, reaching the value equal to that of Pb(II) at 65% at pH 9. Here, the adsorption behaviour of Pb(II) and Cd(II) is

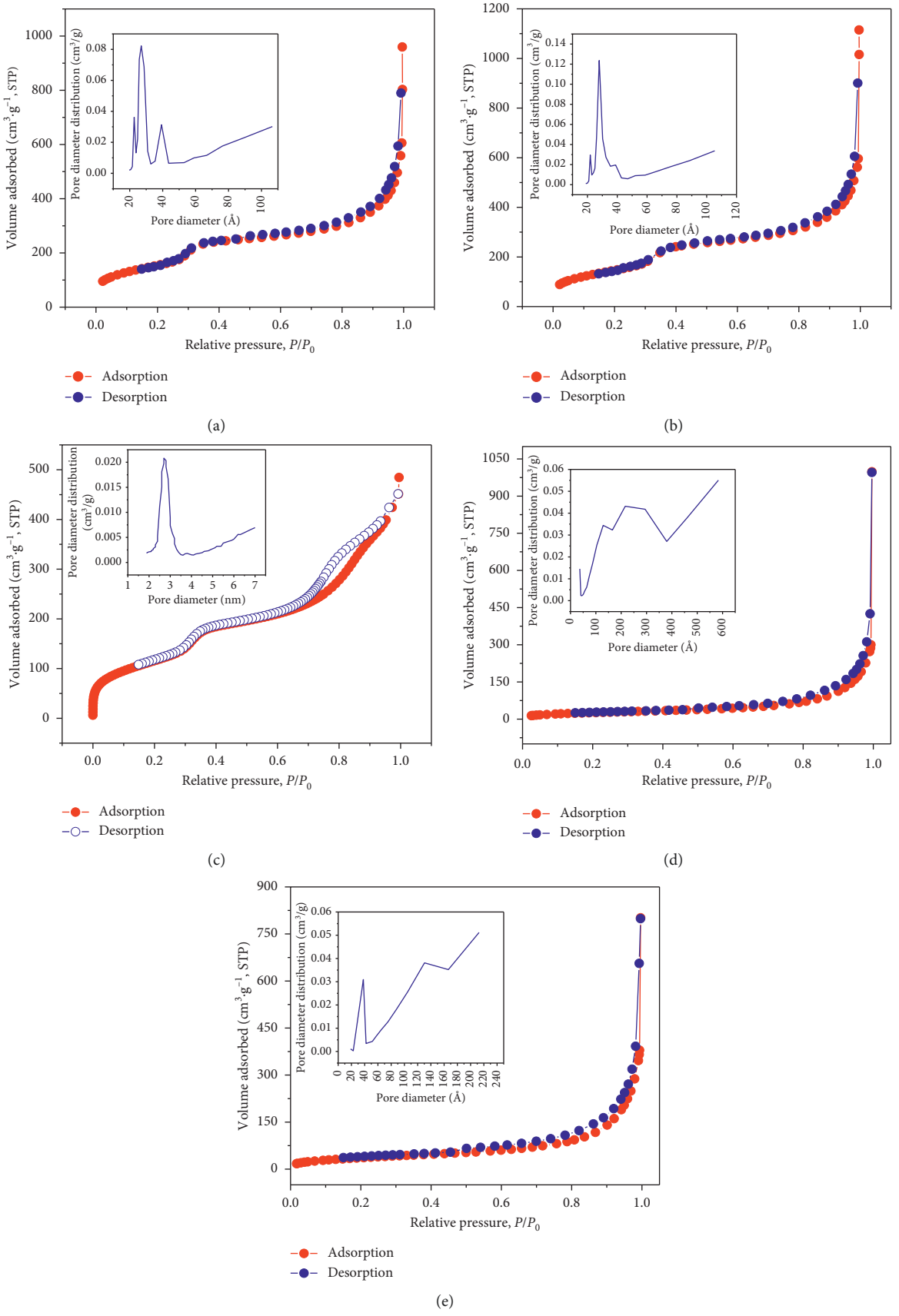


FIGURE 4: Isotherms of nitrogen adsorption/desorption and pore distribution (inset) of MCM-41 and aminopropyl-MCM-41: (a) calcined MCM-41; (b) extracted MCM-41; (c) direct-$NH_2$-MCM-41; (d) post-$NH_2$-calcined MCM-41; (e) post-$NH_2$-extracted MCM-41.

Table 2: Porous properties of MCM-41 and aminopropyl-MCM-41.

| Samples | $d_{(100)}$ (Å) | $a_0$* (Å) | $d_{pore}$ (Å) | $t_w$** (Å) | $S_{BET}$ ($m^2 \cdot g^{-1}$) | $V_{pore}$ ($cm^3 \cdot g^{-1}$) |
|---|---|---|---|---|---|---|
| Calcined MCM-41 | 39.3 | 45.4 | 27.0 | 18.4 | 564 | 1.53 |
| Extracted MCM-41 | 42.5 | 49.1 | 27.9 | 21.2 | 538 | 1.76 |
| Direct-$NH_2$-MCM-41 | 42.1 | 48.6 | 27.0 | 21.6 | 427 | 0.77 |
| Post-$NH_2$-calcined MCM-41 | — | — | — | — | 97 | 1.54 |
| Post-$NH_2$-extracted MCM-41 | — | — | — | — | 137 | 1.01 |

*$a_0 = 2 \cdot (d_{(100)}/\sqrt{3})$; **$t_w = a_0 - d_{pore}$; — N/A.

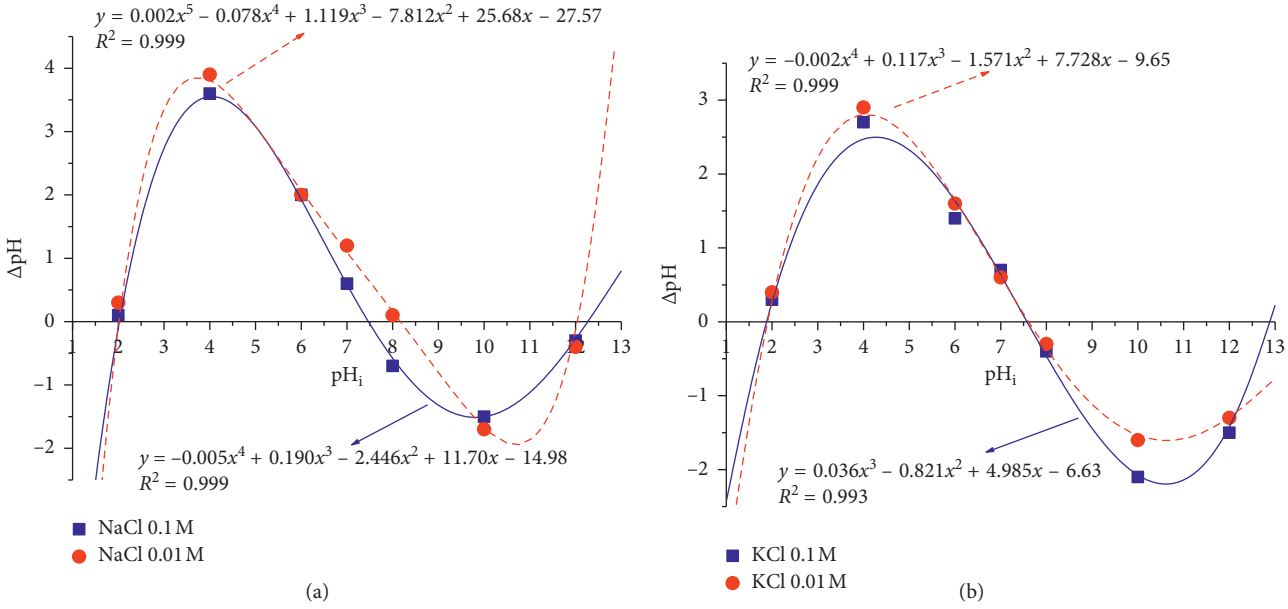


Figure 5: Point of zero charge of the aminopropyl-MCM-41 material in different solutions: (a) NaCl; (b) KCl.

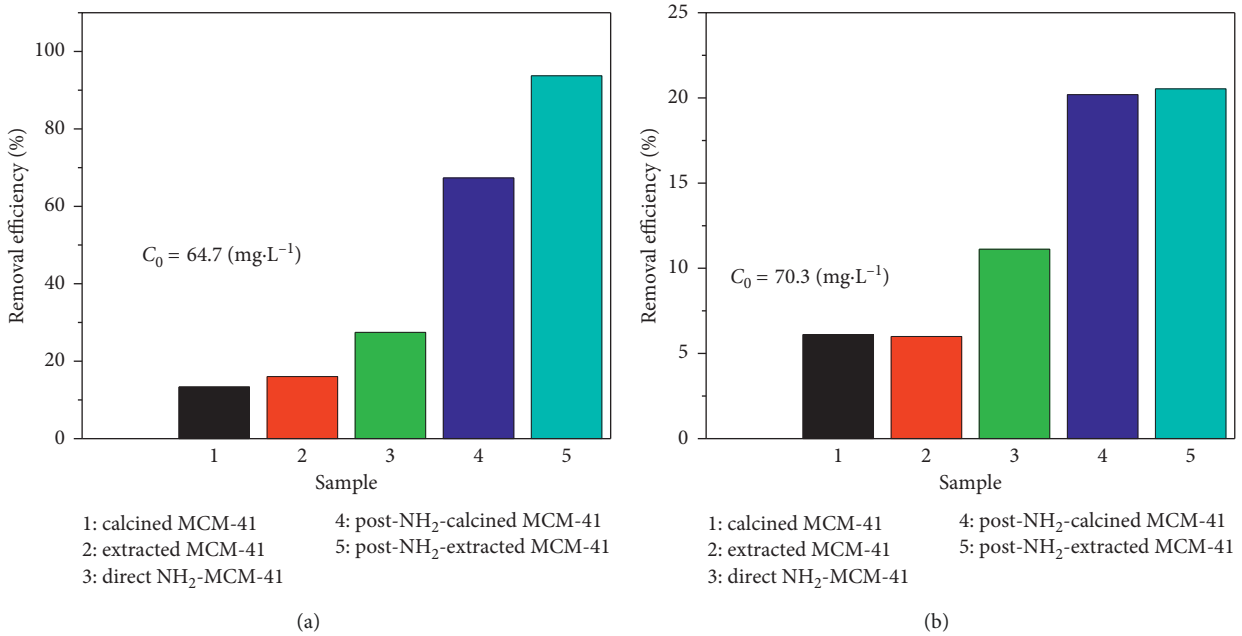


Figure 6: Removal efficiency of heavy metal ions of MCM-41 and aminopropyl-MCM-41: (a) Pb(II); (b) Cd(II) (adsorption condition: $V = 50$ mL, $m = 0.05$ g, room temperature).

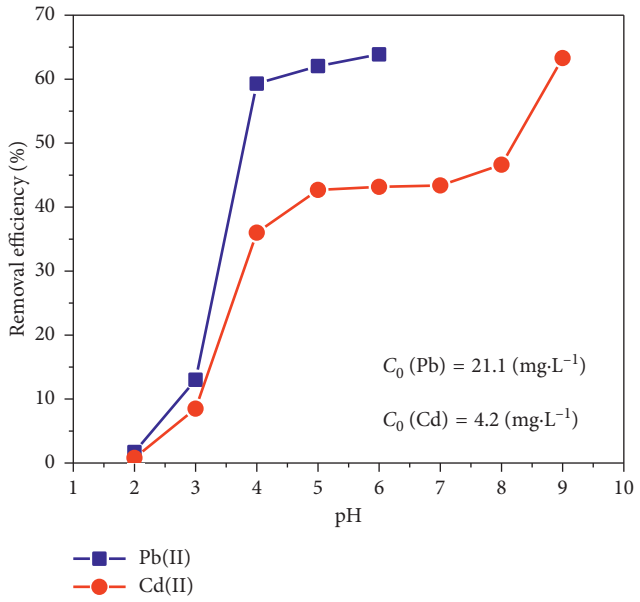


FIGURE 7: Removal efficiency of Pb(II) and Cd(II) ions on post-$NH_2$-extracted MCM-41 at various pH values (adsorption condition: $V = 50$ mL, $m = 0.01$ g, room temperature).

similar to that studied by Heidari et al. [18] on the effect of pH on the adsorption of Pb(II), Cd(II), and Ni(II) on aminopropyl-MCM-41 in the pH range from 1.5 to 5. At pH greater than 6, they proposed that Pb(II) ions precipitated due to a large amount of $OH^-$ ions in the solution when the concentration of the studied ions was very high (50 mg·L$^{-1}$). In our study, the highest pH was 6 for Pb(II) and 9 for Cd(II) with a much lower concentration of metal ions (21.1 mg·L$^{-1}$ for Pb(II) and 4.2 mg·L$^{-1}$ for Cd(II)). In our studied pH range, the metal ions did not precipitate.

The adsorption of Pb(II) and Cd(II) on aminopropyl-MCM-41 in the aqueous solution may occur with the coordination mechanism ($[Me(NH_2)_2]^{2+}$ form, Me is the Pb or Cd ion), as suggested by Benhamou et al. [37]. Besides, the attraction mechanism of the opposite charge between the metal ion and the material surface also takes place. At pH < 5, Pb(II) and Cd(II) ions exist mainly in the $Pb^{2+}$ and $Cd^{2+}$ form. In this pH range, the surface of the aminopropyl-MCM-41 material also has a positive charge (the point of zero charge for the material is ~7.73). At low pH (pH = 2–4), the electrostatic repulsion between $Pb^{2+}$ or $Cd^{2+}$ and the positively charged surface of the material dominates. The adsorption occurs only due to complexation, and this complexation cannot take place significantly because there is also a competition of the $H^+$ ion in the acidic solution. As a result, the removal efficiency is low. In the case of 4 < pH < 6, both the complexation and attraction are dominant as the medium is less acidic with a smaller amount of the $H^+$ ion and less positive material surface, and accordingly, the removal efficiency rises rapidly reaching a high stable value. At pH from 6 to 8, the material surface becomes more or less neutral, and therefore, the adsorption by attraction halts and the efficiency stays practically constant. Further increase of pH makes the surface of the aminopropyl-MCM-41 material become negative, and ionic Cd(II) primarily exists in the $Cd(OH)^+$ form. Thus, the removal efficiency increases significantly again.

*3.2.3. Adsorption Isotherms.* To eliminate errors caused by experimental point [30], typically 4 to 7 experimental points are needed [18, 20, 25, 26, 30, 38, 39]. In this study, 27 experimental points were investigated. The results of the linear regression of the isotherm models, namely, Langmuir, Freundlich, Redlich–Peterson, and Sips, for Pb(II) and Cd(II) adsorption on aminopropyl-MCM-41 are presented in Figure 8 and Table 3.

As a rule, the more the $R^2$ is closer to unity, the more is the model compatible with the experimental data. It is clear from Table 3 that the Langmuir 2 and Redlich–Peterson isotherms fit the experimental data of the adsorption of Pb(II) and Cd(II) the most with $R^2 = 0.999$.

However, the selection of model based on the value of $R^2$ is also biased. For example, in the case of Langmuir 2 and Freundlich equations, if only the linear form is concerned as published in many papers [19, 25–28, 33], where the authors concluded that the Langmuir 2 equation is more appropriate than the Freundlich equation because of its high $R^2$ value. Meanwhile, the Redlich–Peterson equation also has a relatively high coefficient $R^2$.

Recently, many researchers have published their results of nonlinear forms of isotherm equations [18, 21, 25–28]. In this study, the nonlinear forms were also used to compare with the linear forms.

The parameters of the isotherm equations determined with the nonlinear regression method were calculated using the Solver function in Microsoft Excel. In this method, an error function is necessary to match the experimental data in the form of nonlinear isotherm equations. The parameter values are optimised based on the smallest value of this error function. Various error functions have been proposed [21, 23, 33]. In these studies, the error function in the following equation was used [40]:

$$\mathrm{RMSR} = \sqrt{\frac{1}{N} \cdot \sum_{i=1}^{n} \left(q_{e,\exp} - q_{e,\mathrm{cal}}\right)^2}, \tag{11}$$

where RMSR is the root mean squared residual, $q_{e,\exp}$ (mg·g$^{-1}$) is the experimental equilibrium adsorption capacity, $q_{e,\mathrm{cal}}$ (mg·g$^{-1}$) is the calculated equilibrium adsorption capacity, and $N$ is the number of experiments.

The experimental points and the nonlinear regression lines of the adsorption of Pb(II) and Cd(II) ions on aminopropyl-MCM-41 for the models to be compared are shown in Figure 9. The parameters of the models are presented in Table 4.

Table 4 shows that the nonlinear isotherm equations of Langmuir, Redlich–Peterson, and Sips both described quite well the Pb(II) or Cd(II) adsorption on aminopropyl-MCM-41 because the RMSR were small and approximately equal together. Comparisons of $R^2$ in Table 3 with the RMSR error function in Table 4 also show an inconsistence. It is that the

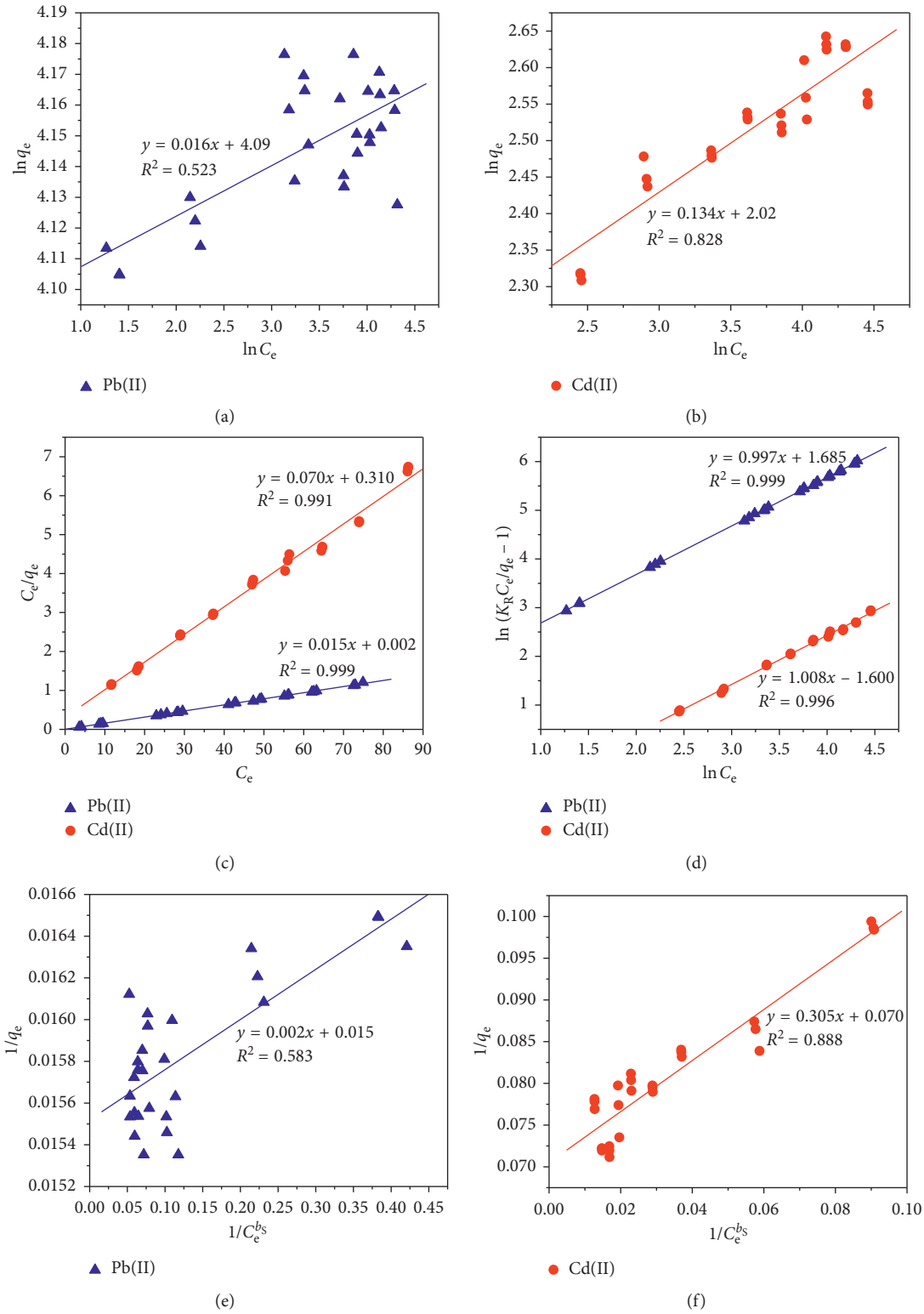


Figure 8: Plots of isotherm equations in a linear form for Pb(II) and Cd(II) adsorption on aminopropyl-MCM-41: (a, b) Freundlich; (c) Langmuir 2; (d) Redlich–Peterson; (e, f) Sips's model (adsorption condition: $V = 50$ mL, $m = 0.05$ g, room temperature).

$R^2$ value of the Sips equation was very low, while the RMSR of the one in the nonlinear form was very small. This is also evidence of a limitation using the value of error functions to assess model compatibility.

The majority of works published on assessing the compatibility of the model are based on the value of the error function. If the error function value of the model is the smallest, the model is the most compatible. It is also

Table 3: Parameters of the isotherm equations determined by using the linear form of Pb(II) and Cd(II) adsorption on aminopropyl-MCM-41.

| Ion | Isotherm (linear form) | $q_m$ (mg·g$^{-1}$) | $K_L$, $K_F$, $K_R$, or $K_{S2}$ | $a_R$ or $a_S$ | $n$, $b_R$, or $b_S$ | $R^2$ |
|---|---|---|---|---|---|---|
| Pb(II) | Langmuir 1 | 66.66 | 5.00 | — | — | 0.574 |
| | Langmuir 2 | 66.66 | 7.50 | — | — | **0.999** |
| | Langmuir 3 | 63.99 | 4.67 | — | — | 0.552 |
| | Langmuir 4 | 64.64 | 2.57 | — | — | 0.552 |
| | Langmuir 5 | 64.56 | 2.64 | — | — | 0.574 |
| | Freundlich | — | 59.73 | — | 62.50 | 0.523 |
| | Redlich–Peterson | — | 341.86 | 5.39 | 0.99 | **0.999** |
| | Sips | — | 500.00 | 7.50 | 0.68 | 0.583 |
| Cd(II) | Langmuir 1 | 14.28 | 0.21 | — | — | 0.888 |
| | Langmuir 2 | 14.28 | 0.22 | — | — | **0.991** |
| | Langmuir 3 | 14.13 | 0.22 | — | — | 0.815 |
| | Langmuir 4 | 14.54 | 0.18 | — | — | 0.815 |
| | Langmuir 5 | 14.40 | 0.19 | — | — | 0.888 |
| | Freundlich | — | 7.58 | — | 7.46 | 0.828 |
| | Redlich–Peterson | — | 2.96 | 0.20 | 1.00 | **0.996** |
| | Sips | — | 3.27 | 0.22 | 0.97 | 0.888 |

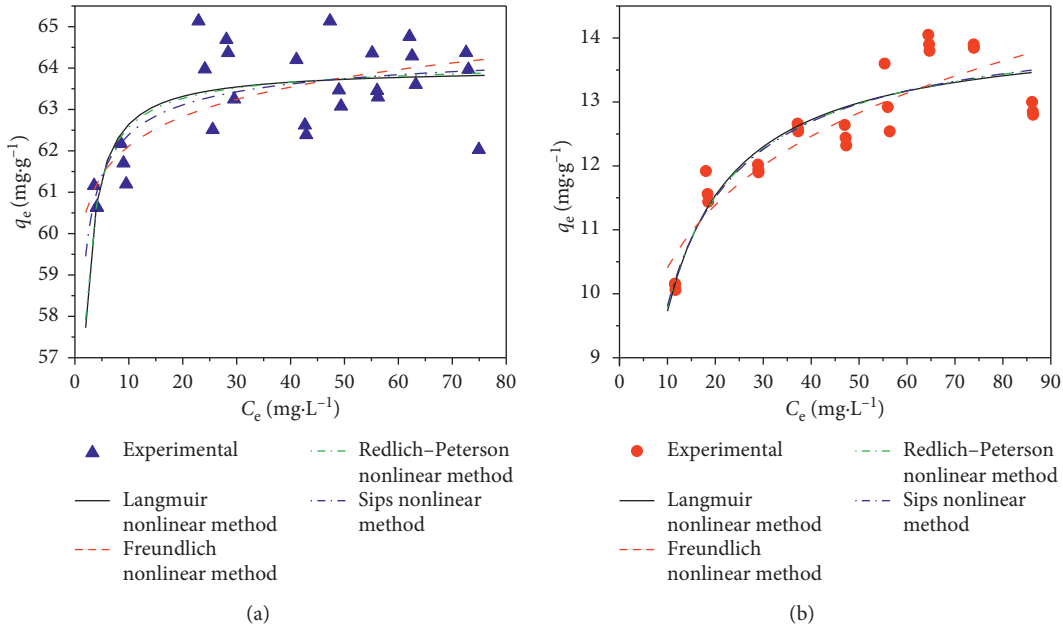


Figure 9: Adsorption isotherms determined using the nonlinear method for the adsorption of metal ions onto aminopropyl-MCM-41: (a) Pb(II); (b) Cd(II) (adsorption condition: $V = 50$ mL, $m = 0.05$ g, room temperature).

unreasonable because the difference is probably due to random errors. There have never been works that had made a statistical error function to indicate a certain error value. If the value of the error calculation results is larger or smaller than this value, the model accepted to be compatible with experimental data. So, how to know which models are described equally well with experimental data? All proposed error functions [21, 23, 31, 33] do not solve the problem because the error functions are not statistical functions. Thus, it needs to seek an error function that has a statistically normal distribution function to solve this problem.

The general principles of the evaluation model can be interpreted as follows: a set of adsorption capacity data from experimental equilibrium ($q_{e,exp}$) via a certain model will change a set value $q_{e,cal}$, as illustrated in Figure 10.

The model is the most appropriate if the difference between $q_{e,exp}$ and $q_{e,cal}$ is smallest. All error functions are based on this principle [21, 23, 31, 33]. On this basis, we believe that the most appropriate model is the one to create the $q_{e,cal}$ values that have the same sampling distribution as the $q_{e,exp}$ values, or in the other words, the average capacity calculated from the model is the closest to the average experimental capacity. We used the paired-samples $t$-test for

Table 4: Regression parameters of the different nonlinear isotherm models for the adsorption of Pb(II) and Cd(II) on aminopropyl-MCM-41.

| Ion | Isotherm (nonlinear form) | $q_m$ (mg·g$^{-1}$) | $K_L$, $K_F$, $K_R$, or $K_{S2}$ | $a_R$ or $a_S$ | $n$, $b_R$, or $b_S$ | RMSR |
|---|---|---|---|---|---|---|
| Pb(II) | Langmuir | 64.00 | 4.59 | — | — | 0.877 |
| | Freundlich | — | 59.82 | — | 61.28 | 0.924 |
| | Redlich–Peterson | — | 322.15 | 5.06 | 0.99 | 0.876 |
| | Sips | — | 499.98 | 7.71 | 0.52 | 0.876 |
| Cd(II) | Langmuir | 14.17 | 0.21 | — | — | 0.440 |
| | Freundlich | — | 7.71 | — | 7.68 | 0.490 |
| | Redlich–Peterson | — | 3.37 | 0.25 | 0.98 | 0.440 |
| | Sips | — | 3.94 | 0.27 | 0.88 | 0.439 |

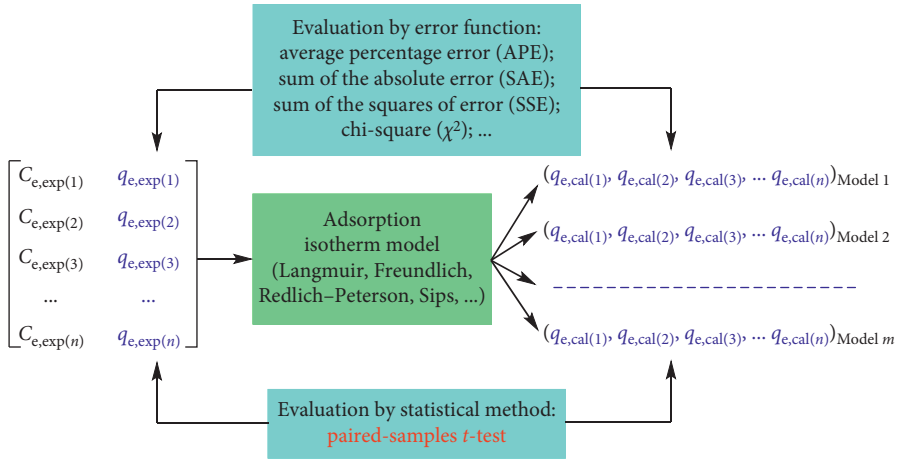


Figure 10: Idea of the statistical evaluation of the adsorption isotherm model.

this assessment. The value of the statistical $t$-test is calculated according to Field as follows [41]:

$$t = \frac{\sum d}{\sqrt{\left(N \cdot \left(\sum d^2\right) - \left(\sum d\right)^2\right)/(N-1)}}, \quad (12)$$

where $d$ is the difference of the compared pairs ($d = q_{e,exp} - q_{e,cal}$) and $N$ is the total number of pairs.

To apply this comparison, the sequence of $q_{e,cal}$ and $q_{e,exp}$ should meet the testing hypotheses: (i) dependent assumption: the values of $q_{e,cal}$ and $q_{e,exp}$ combine pairs together because they are calculated from starting values of $q_{e,exp}$, and this assumption is satisfied; (ii) normally distributed assumption, it mean difference scores are normally distributed in the population, or there is a large sample size (approximately 30): in this case, because of the large sample size ($N = 27$), the condition is satisfied [41]; and (iii) dependent variable assumption is at least the variable interval: this condition is also satisfied.

$H_0$ hypothesis: the average value of $q_{e,cal}$ is not different from the average value of $q_{e,exp}$. This means that the model gives a goodness description of the experimental data.

In software, such as Microsoft Excel or SPSS, the statistical values of $t$ are transferred to corresponding probability values of $p$. $p$ is the probability at which people can trust that the $H_0$ hypothesis is correct. For statistical comparisons, the level of significance $\alpha$ must be set first. This level is optional and often chosen at 0.05, 0.01, or 0.001 to evaluate the difference between the two compared quantities. In this study, the comparative expectation of the two number sequences is the same, so we selected $\alpha = 0.95$. This means that we are 95% confident that the $H_0$ hypothesis is true. If $p > 0.95$ then $H_0$ is accepted, and therefore, the average value of $q_{e,cal}$ is not different from that of $q_{e,exp}$ at the statistically significant level $\alpha = 0.95$, or the model is accepted. Conversely, if $p < 0.95$, then the $H_0$ hypothesis is rejected, and the model is not accepted.

The data are analysed with the paired-samples $t$-test at $\alpha = 0.95$ using the SPSS-17 software (Statistical Package for the Social Sciences). For the adsorption of Pb(II), 6 equations had $p < 0.95$, indicating that there was a statistically significant difference in the equilibrium adsorption capacity values given by the equation and the experimental data; 6 remaining equations, Langmuir 3, Langmuir 5, Langmuir nonlinear, Freundlich nonlinear, Redlich–Peterson nonlinear, and Sips nonlinear had $p > 0.95$ (Table 5) and should not have the statistically significant differences between the mean values of $q_{e,cal}$ and $q_{e,exp}$. Therefore, these 6 equations appropriately describe the experimental data at $\alpha = 0.95$.

Similarly, the results of the paired-samples $t$-test for adsorption of Cd(II) showed that four equations in the nonlinear forms, namely, Redlich–Peterson, Sips, Langmuir,

Table 5: Results of the paired-samples $t$-test analysis of adsorption of Pb(II) and Cd(II) on aminopropyl-MCM-41.

| For adsorption of Pb(II) | | | For adsorption of Cd(II) | | |
|---|---|---|---|---|---|
| *Isotherm* | *t* | *p* | *Isotherm* | *t* | *p* |
| Langmuir (nonlinear) | 0.001 | **1.000** | Redlich–Peterson (nonlinear) | 0.001 | **1.000** |
| Freundlich (nonlinear) | 0.001 | **1.000** | Sips (nonlinear) | 0.001 | **1.000** |
| Redlich–Peterson (nonlinear) | −0.014 | **0.989** | Langmuir (nonlinear) | 0.002 | **0.999** |
| Sips (nonlinear) | −0.014 | **0.989** | Freundlich (nonlinear) | −0.007 | **0.994** |
| Langmuir 3 | 0.013 | **0.989** | Langmuir 3 | 0.095 | 0.925 |
| Langmuir 5 | 0.061 | **0.952** | Redlich–Peterson (linear) | 0.101 | 0.920 |
| Langmuir 4 | −0.139 | 0.891 | Langmuir 5 | −0.221 | 0.827 |
| Redlich–Peterson (linear) | −0.848 | 0.404 | Freundlich (linear) | 0.299 | 0.767 |
| Freundlich (linear) | 0.896 | 0.379 | Langmuir 4 | −0.463 | 0.647 |
| Langmuir 1 | −15.632 | <0.001 | Sips (linear) | −0.781 | 0.442 |
| Langmuir 2 | −15.921 | <0.001 | Langmuir 1 | −1.179 | 0.249 |
| Sips (linear) | −13.671 | <0.001 | Langmuir 2 | −1.641 | 0.113 |

Table 6: A comparison of Pb(II) and Cd(II) adsorption capacity of aminopropyl-MCM-41 with some other published adsorbents.

| Adsorbent | Adsorption capacity ($mg \cdot g^{-1}$) | | References |
|---|---|---|---|
| | Pb(II) | Cd(II) | |
| Aminopropyl-MCM-41 | 64.21 | 14.08 | The present work |
| $NH_2$-MCM-41 | 57.7 | 18.2 | [18] |
| Amino-modified silica aerogel | 45.45 | 35.71 | [42] |
| Amino-functionalized magnetite/kaolin clay | 86.1 | 22.1 | [43] |
| Silicalite-I-$NH_2$ | 43.5 | — | [44] |
| MCM-48-$NH_2$ | 75.2 | — | [44] |
| MCM-48-SH | 31.2 | — | [44] |
| Soil amendment | — | 7.47–17.67 | [45] |
| Dithizone-modified bagasse | 37.20 | — | [46] |
| Chromium-doped nickel nanometal oxide | 1.7914 | 5.243 | [47] |

and Freundlich, had $p > 0.95$, revealing that these models are the appropriate description for the experimental data at $\alpha = 0.95$.

Hence, in terms of statistics, the four nonlinear models, namely, Langmuir, Freundlich, Redlich–Peterson, and Sips, most appropriately described the adsorption data of Pb(II) and Cd(II) on aminopropyl-MCM-41. This also confirms that nonlinear equations have matched the results more than linear equations in this study. This result is consistent with that of other works [25–28].

The maximum adsorption capacity of the aminopropyl-MCM-41 material calculated from the various compatibility equations (Langmuir 3, Langmuir 5, Langmuir model in the nonlinear form, Freundlich in the nonlinear form, Redlich–Peterson in the nonlinear form, and Sips in the nonlinear form for the adsorption of Pb(II); and Langmuir in the nonlinear form, Freundlich in the nonlinear form, Redlich–Peterson nonlinear, and Sips in the nonlinear form for the adsorption of Cd(II)) was 64.21 $mg \cdot g^{-1}$ ($N = 5$, SE = 0.21) for Pb(II) and 14.08 $mg \cdot g^{-1}$ ($N = 3$, SE = 0.33) for Cd(II). The small standard error proves the correctness of the paired-samples $t$-test method.

The adsorption capacity in this work was compared with the results reported previously [18, 42–47]. A comparison was listed in Table 6. It could be noticed that the adsorption capacity was higher or comparable within previous papers. The aminopropyl-MCM-41 exhibited better than some of the adsorbent based on MCM-48, silicalite-1, or chromium-doped nickel nanometal oxide but failed to some others.

## 4. Conclusions

A comparison of physicochemical characteristics of aminopropyl-MCM-41 prepared via direct and postsynthesis was performed. The aminopropyl-MCM-41 material prepared by means of the direct process exhibits good porous properties but low aminopropyl loading compared with the samples prepared via postsynthesis. Parent MCM-41 remarkably affects the physicochemical properties of resulting aminopropyl-MCM-41. The extracted MCM-41 material gave higher aminopropyl loading and better porous properties than the calcined MCM-41 counterpart, and therefore, it provided a high adsorption capacity for Pb(II) and Cd(II) at 64.21 $mg \cdot g^{-1}$ and 14.08 $mg \cdot g^{-1}$, respectively. The paired-samples $t$-test could eliminate the part-sided assessment based on the minimum value of the error function. According to our knowledge, this is the first study applying the statistical test to assess the compatibility of the isothermal models in terms of theory as well as practice.

## Data Availability

The data used to support the findings of this study are available from the corresponding author upon request.

## Conflicts of Interest

The authors declare that they have no conflicts of interest.

## References


[1] A. T. Paulino, L. B. Santos, and J. Nozaki, "Removal of $Pb^{2+}$, $Cu^{2+}$, and $Fe^{3+}$ from battery manufacture wastewater by chitosan produced from silkworm chrysalides as a low-cost adsorbent," *Reactive and Functional Polymer*, vol. 62, no. 2, pp. 634–642, 2008.

[2] Agency for Toxic Substances and Disease Registry, *Toxicological Profile for Polycyclic Aromatic Hydrocarbons*, U.S. Department of Health & Human Services, Public Health Service, Agency for Toxic Substances and Disease Registry, Washington, DC, USA, 1999.

[3] J. Pan, J. A. Plant, N. Voulvoulis, C. J. Oates, and C. Ihlenfeld, "Cadmium levels in Europe: implications for human health," *Environmental Geochemistry and Health*, vol. 32, no. 1, pp. 1–12, 2010.

[4] H. J. Mansoorian, A. H. Mahvi, and A. J. Jafari, "Removal of lead and zinc from battery industry wastewater using electrocoagulation process: influence of direct and alternating current by using iron and stainless steel rod electrodes," *Separation and Purification Technology*, vol. 135, pp. 165–175, 2014.

[5] T. Mahmood, M. T. Saddique, A. Naeem, S. Mustafa, B. Dilara, and Z. A. Raza, "Cation exchange removal of Cd from aqueous solution by NiO," *Journal of Hazardous Materials*, vol. 185, no. 2-3, pp. 824–828, 2011.

[6] N. Pont, V. Salvadó, and C. Fontàs, "Selective transport and removal of Cd from chloride solutions by polymer inclusion membranes," *Journal of Membrane Science*, vol. 318, no. 1-2, pp. 340–345, 2008.

[7] C. T. Kresge and W. J. Roth, "The discovery of mesoporous molecular sieves from the twenty year perspective," *Chemical Society Reviews*, vol. 42, no. 9, pp. 3663–3670, 2013.

[8] R. Köhn, D. Paneva, M. Dimitrov et al., "Studies on the state of iron oxide nanoparticles in MCM-41 and MCM-48 silica materials," *Microporous and Mesoporous Materials*, vol. 63, no. 1–3, pp. 125–137, 2003.

[9] L. C. Juang, C. C. Wang, and C. K. Lee, "Adsorption of basic dyes onto MCM-41," *Chemosphere*, vol. 64, no. 11, pp. 1920–1928, 2006.

[10] M. Anbia and M. Lashgari, "Synthesis of amino-modified ordered mesoporous silica as a new nano sorbent for the removal of chlorophenols from aqueous media," *Chemical Engineering Journal*, vol. 150, no. 2-3, pp. 555–560, 2009.

[11] G. L. Athens, R. M. Shayib, and B. F. Chmelka, "Functionalization of mesostructured inorganic-organic and porous inorganic materials," *Current Opinion in Colloid and Interface Science*, vol. 14, no. 4, pp. 281–292, 2009.

[12] A. Deryło-Marczewska, M. Zienkiewicz-Strzałka, K. Skrzypczyńska, A. Świątkowski, and K. Kuśmierek, "Evaluation of the SBA-15 materials ability to accumulation of 4-chlorophenol on carbon paste electrode," *Adsorption*, vol. 22, no. 4–6, pp. 801–812, 2016.

[13] A. Arencibia, J. Aguado, and J. M. Arsuaga, "Regeneration of thiol-functionalized mesostructured silica adsorbents of mercury," *Applied Surface Science*, vol. 256, no. 17, pp. 5453–5457, 2010.

[14] H. Sepehrian, S. Waqif-Husain, and M. Ghannadi-Maragheh, "Development of thiol-functionalized mesoporous silicate MCM-41 as a modified sorbent and its use in chromatographic separation of metal ions from aqueous nuclear waste," *Chromatographia*, vol. 70, no. 1-2, pp. 277–280, 2009.

[15] T. M. Suzuki, T. Nakamura, K. Fukumoto, M. Yamamoto, Y. Akimoto, and K. Yano, "Direct synthesis of amino-functionalized monodispersed mesoporous silica spheres and their catalytic activity for nitroaldol condensation," *Journal of Molecular Catalysis A: Chemical*, vol. 280, no. 1-2, pp. 224–232, 2008.

[16] S. Wu, F. Li, R. Xu, S. Wei, and G. Li, "Synthesis of thiol-functionalized MCM-41 mesoporous silicas and its application in Cu(II), Pb(II), Ag(I), and Cr(III) removal," *Journal of Nanoparticle Research*, vol. 12, no. 6, pp. 2111–2124, 2010.

[17] K. M. Parida and D. Rath, "Amine functionalized MCM-41: an active and reusable catalyst for Knoevenagel condensation reaction," *Journal of Molecular Catalysis A: Chemical*, vol. 310, no. 1-2, pp. 93–100, 2009.

[18] A. Heidari, H. Younesi, and Z. Mehraban, "Removal of Ni(II), Cd(II), and Pb(II) from a ternary aqueous solution by amino functionalized mesoporous and nano mesoporous silica," *Chemical Engineering Journal*, vol. 153, no. 1–3, pp. 70–79, 2009.

[19] J. Aguado, J. M. Arsuaga, A. Arencibia, M. Lindo, and V. Gascón, "Aqueous heavy metals removal by adsorption on amine-functionalized mesoporous silica," *Journal of Hazardous Materials*, vol. 163, no. 1, pp. 213–221, 2009.

[20] B. H. Hameed, A. A. Ahmad, and N. Aziz, "Isotherms, kinetics and thermodynamics of acid dye adsorption on activated palm ash," *Chemical Engineering Journal*, vol. 133, no. 1–3, pp. 195–203, 2007.

[21] O. Hamdaoui and E. Naffrechoux, "Modeling of adsorption isotherms of phenol and chlorophenols onto granular activated carbon. Part I. Two-parameter models and equations allowing determination of thermodynamic parameters," *Journal of Hazardous Material*, vol. 147, no. 1-2, pp. 381–394, 2007.

[22] O. Hamdaoui and E. Naffrechoux, "Modeling of adsorption isotherms of phenol and chlorophenols onto granular activated carbon. Part II. Models with more than two parameters," *Journal of Hazardous Materials*, vol. 147, no. 1-2, pp. 401–411, 2007.

[23] S. J. Allen, Q. Gan, R. Matthews, and P. A. Johnson, "Comparison of optimised isotherm models for basic dye adsorption by kudzu," *Bioresource Technology*, vol. 88, no. 2, pp. 143–152, 2003.

[24] A. Kumar, B. Prasad, and I. M. Mishra, "Adsorptive removal of acrylonitrile by commercial grade activated carbon: kinetics, equilibrium and thermodynamics," *Journal of Hazardous Materials*, vol. 152, no. 2, pp. 589–600, 2008.

[25] K. V. Kumar and S. Sivanesan, "Comparison of linear and non-linear method in estimating the sorption isotherm parameters for safranin onto activated carbon," *Journal of Hazardous Materials*, vol. 123, no. 1–3, pp. 288–292, 2005.

[26] K. V. Kumar and S. Sivanesan, "Prediction of optimum sorption isotherm: comparison of linear and non-linear method," *Journal of Hazardous Materials*, vol. 126, no. 1–3, pp. 198–201, 2005.

[27] K. Vasanth Kumar and S. Sivanesan, "Isotherms for Malachite Green onto rubber wood (*Hevea brasiliensis*) sawdust: comparison of linear and non-linear methods," *Dyes and Pigments*, vol. 72, no. 1, pp. 124–129, 2007.

[28] K. Vasanth Kumar and S. Sivanesan, "Sorption isotherm for safranin onto rice husk: comparison of linear and non-linear methods," *Dyes and Pigments*, vol. 72, no. 1, pp. 130–133, 2007.

[29] Y. S. Ho, W. T. Chiu, and C. C. Wang, "Regression analysis for the sorption isotherms of basic dyes on sugarcane dust," *Bioresource Technology*, vol. 96, no. 11, pp. 1285–1291, 2005.

[30] M. I. El-Khaiary and G. F. Malash, "Common data analysis errors in batch adsorption studies," *Hydrometallurgy*, vol. 105, no. 3-4, pp. 314–320, 2011.

[31] Y. C. Wong, Y. S. Szeto, W. H. Cheung, and G. McKay, "Adsorption of acid dyes on chitosan—equilibrium isotherm analyses," *Process Biochemistry*, vol. 39, no. 6, pp. 695–704, 2004.

[32] B. H. Dang Son, V. Quang Mai, D. Xuan Du, N. Hai Phong, and D. Quang Khieu, "A study on astrazon black AFDL dye adsorption onto Vietnamese diatomite," *Journal of Chemistry*, vol. 2016, Article ID 8685437, 11 pages, 2016.

[33] K. Y. Foo and B. H. Hameed, "Insights into the modeling of adsorption isotherm systems," *Chemical Engineering Journal*, vol. 156, no. 1, pp. 2–10, 2010.

[34] A. Ortlam, J. Rathouský, G. Schulz-Ekloff, and A. Zukal, "MCM-41 as-synthesized and calcined materials: temporal development of X-ray reflection intensity and pore volume," *Microporous Materials*, vol. 6, no. 4, pp. 171–180, 1996.

[35] M. Kosmulski, "pH-dependent surface charging and points of zero charge II. Update," *Journal of Colloid and Interface Science*, vol. 275, no. 1, pp. 214–224, 2004.

[36] Q. Qin, J. Ma, and K. Liu, "Adsorption of anionic dyes on ammonium-functionalized MCM-41," *Journal of Hazardous Materials*, vol. 162, no. 1, pp. 133–139, 2009.

[37] A. Benhamou, M. Baudu, Z. Derriche, and J. P. Basly, "Aqueous heavy metals removal on amine-functionalized Si-MCM-41 and Si-MCM-48," *Journal of Hazardous Materials*, vol. 171, no. 1–3, pp. 1001–1008, 2009.

[38] N. D. V. Quyen, T. N. Tuyen, D. Q. Khieu et al., "Lead ions removal from aqueous solution using modified carbon nanotubes," *Bulletin of Materials Science*, vol. 41, p. 6, 2018.

[39] N. T. V. Hoan, N. T. A. Thu, H. Van Duc, N. D. Cuong, D. Q. Khieu, and V. Vo, "$Fe_3O_4$/reduced graphene oxide nanocomposite: synthesis and its application for toxic metal ion removal," *Journal of Chemistry*, vol. 2016, Article ID 2418172, 10 pages, 2016.

[40] K. P. Singh, N. Basant, A. Malik, and G. Jain, "Modeling the performance of 'up-flow anaerobic sludge blanket' reactor based wastewater treatment plant using linear and nonlinear approaches—a case study," *Analytica Chimica Acta*, vol. 658, no. 1, pp. 1–11, 2010.

[41] A. Field, *Discovering Statistics Using SPSS*, SAGE Publishing, Thousand Oaks, CA, USA, 2010.

[42] H. Faghihian, H. Nourmoradi, and M. Shokouhi, "Performance of silica aerogels modified with amino functional groups in Pb(II) and Cd(II) removal from aqueous solutions," *Polish Journal of Chemical Technology*, vol. 14, no. 1, pp. 50–56, 2012.

[43] L. Qin, L. Yan, J. Chen, T. Liu, H. Yu, and B. Du, "Enhanced removal of $Pb^{2+}$, $Cu^{2+}$, and $Cd^{2+}$ by amino-functionalized magnetite/kaolin clay," *Industrial & Engineering Chemistry Research*, vol. 55, no. 27, pp. 7344–7354, 2016.

[44] A. A. Malhis, S. H. Arar, M. K. Fayyad, and H. A. Hodali, "Amino- and thiol-modified microporous silicalite-1 and mesoporous MCM-48 materials as potential effective adsorbents for Pb(II) in polluted aquatic systems," *Adsorption Science & Technology*, vol. 36, no. 1-2, pp. 270–286, 2018.

[45] S. Li, M. Wang, Z. Zhao, C. Ma, and S. Chen, "Adsorption and desorption of Cd by soil amendment: mechanisms and environmental implications in Field-Soil remediation," *Sustainability*, vol. 10, no. 7, p. 2337, 2018.

[46] R. Shiralipour and T. Hamoule, "Removal of Pb(II) from contaminated water by bagasse adsorbent modified with dithizone," *Jundishapur Journal of Health Sciences*, vol. 10, no. 3, p. e62360, 2018.

[47] Y. V. S. Sai Krishna, G. Sandhya, and R. Ravichandra Babu, "Removal of heavy metals Pb(II), Cd(II) and Cu(II) from waste waters using synthesized chromium doped nickel oxide nano particles," *Bulletin of the Chemical Society of Ethiopia*, vol. 32, no. 2, pp. 225–238, 2018.